Published in final edited form as:
Bioelectromagnetics. 2013 January ; 34(1): 22–30. doi:10.1002/bem.21741.

Electric Fields Caused by Blood Flow Modulate Vascular Endothelial Electrophysiology and Nitric Oxide Production

Darshan P. Trivedi[1], **Kevin J. Hallock**[1], and **Peter R. Bergethon**[1,2]

[1]Department of Anatomy and Neurobiology, Boston University School of Medicine, Laboratory for Intelligence Modeling and Neurophysics

[2]Department of Biochemistry, Boston University School of Medicine, Laboratory for Intelligence Modeling and Neurophysics

Abstract

Endothelial cells are exposed to a ubiquitous, yet unexamined electrical force caused by blood flow: the electrokinetic vascular streaming potential (EVSP). In this study, the hypothesis that extremely low frequency (ELF) electric fields parameterized by the EVSP have significant biological effects on endothelial cell properties was studied by measuring membrane potential and nitric oxide production under ELF stimulation between 0–2 Hz and 0–6.67 volts per meter. Using membrane potential and nitric oxide sensitive fluorescent dyes, bovine aortic endothelial cells (BAECs) in culture were studied in the presence and absence of EVSP-modeled electric fields. The transmembrane potential of BAECs was shown to depolarize between 1–7 mV with a strong dependency on both the magnitude and frequency of the isolated ELF field. The findings also support a field interaction with a frequency-dependent tuning curve. The ELF field complexly modulates the nitric oxide response to adenosine triphosphate stimulation with potentiation seen with up to a seven-fold increase. This potentiation was also frequency and magnitude dependent. An early logarithmic phase of NO production is enhanced in a field strength- dependent manner, but the ELF field does not modify a later exponential phase. This study shows that using electric fields on the order of those generated by blood flow influences the essential biology of endothelial cells. The inclusion of ELF electric fields in the paradigm of vascular biology may create novel opportunities for advancing both the understanding and therapies for treatment of vascular diseases.

Keywords

streaming potential; electrokinetics; membrane potential; vascular endothelium

INTRODUCTION

The human impact of atherosclerotic and hypertensive vascular disease throughout the world is staggering. The spawn of these processes, heart disease and stroke, are responsible for worldwide death rates of 1 person every 2.3 s while every 6.3 s someone is permanently disabled by a stroke [Roger et al., 2011; WHO, 2011]. The normal biology of the vascular system involves a complex interaction between cells, the extracellular matrix (ECM), blood, and mechanical forces [Schwartz et al., 1991]. The current thinking about vascular

Address correspondence to: Peter R. Bergethon, Laboratory for Intelligence Modeling and Neurophysics, Department of Anatomy and Neurobiology, Boston University School of Medicine, 650 Albany Street, Boston, MA 02118, prberget@bu.edu, 617-638-4108 (office), 617-414-2329 (FAX).

Disclosures: The authors have nothing to disclose.

pathobiology focuses on the role played by lipids, inflammatory cells, enzymes that modify the ECM, and responses to mechanical stresses [Cunningham and Gotlieb, 2005; Falk, 2006]. Blood flow causes mechanical stress (shearing, tensile, compressive) on the blood vessel components including the endothelial and smooth muscle cells, with many aspects of normative and pathobiology responding to these mechanical forces [Li et al., 2005].

Blood flow also produces a concomitant electrical force that acts within the blood vessel–the electrokinetic vascular streaming potential (EVSP). Though the phenomenon of the streaming potential has been known since Quincke first described it in 1861, its potential biological role in the vascular system was demonstrated only in recent decades [Bergethon, 1991]. Sawyer and coworkers [1966] investigated the role of electrokinetic processes as a factor in hemostasis and measured the streaming potential in live animals. They established the magnitude of the EVSP between 0.7 V/m and 3.0 V/m. Bergethon [1991] developed a simple model for field calculation based on the classical derivation of the EVSP as described by the Helmholtz-Smoluchowski equation with a correction for pulsatile flow ($f(Ya)$): $Es = [\zeta\varepsilon\varepsilon_0 P/\eta\kappa]\ (f(Ya))$, where Es is the streaming potential (volts), ζ is the zeta potential (volts) of the vessel, ε is the dielectric constant of the electrolyte, ε_0 is the permittivity of free space, P is the effective systolic pressure in N-m^{-2}, η is the electrolyte viscosity in kg-m^{-1}-s^{-1}, and κ is the conductivity in S-m^{-1}. The correction for pulsatile flow, $f(Ya)$, came after Packard [1953] used a Bessel function for (Ya) and determined that at the frequencies and dimensions of the bovine aortic system, the value of $f(Ya)$ is 1.0. The modeled field, Es, is time varying with a sinusoidal form. *In vivo*, the EVSP is produced by mechanical events that also generate shear and normal tensile mechanical forces in the vessel; therefore, an essential design aspect of the EVSP effects require the isolated application of extremely low frequency (ELF) electric forces without any mechanical stimulus. Application of these isolated EVSP-type ELF fields on vascular smooth muscle cells have been shown to have a biologically relevant impact on the electrophysiology and electro-pharmacology of the vascular smooth muscle cell [Bergethon, 1991].

Most stimuli that act at the vascular endothelial cell surface, including mechanotransduction and chemical action, cause the release of endothelium-dependent vasodilators secondary to an increase in intracellular Ca^{2+} [Adams et al., 1989; Noris et al., 1995]. The most common of these is nitric oxide (NO). The intracellular increase in calcium occurs either from Ca^{2+} influx or from an inositol triphosphate (IP_3)-mediated release of Ca^{2+} from intracellular stores. The rise in intracellular Ca^{2+} activates NO synthase, producing NO and activating Ca^{2+}-dependent K^+ channels that lead to hyperpolarization of the endothelial cells. More Ca^{2+} flows across this electrical gradient into the cell, thus sustaining the production of these vasoactive substances. Given this background it was reasoned that independent regulation of vascular endothelial cell biology by similar ELF fields would be demonstrated by alterations in the variables of transmembrane potential and NO production.

MATERIAL AND METHODS

Cell Culture of Bovine Aortic Endothelial Cells

All experiments in this study were performed using bovine aortic endothelial cells (BAECs) purchased from Cell Systems (#CSC-2B2, CSC, Seattle, WA) and were cultured according to the method of Augustin-Voss et al. [1993], modified by the addition of 1 mM ascorbic acid and 0.01% dimethyl sulfoxide to the culture media. Cell culture solutions (Gibco brand) were purchased from Life Technologies (Carlsbad, CA), except fetal bovine serum (FBS; #S11550, Atlanta Biologicals, Atlanta, GA). Surfaces on which BAECs were grown were coated with a 0.1% gelatin in 0.1 mol/l phosphate buffered saline (PBS) solution one day prior to cell seeding. The cells were passaged into a gelatin-coated T75 flask. Cultures were

assessed daily with phase microscopy for confluence, which typically occurred after four days, yielding approximately 1.5×10^6 cells/flask.

For the experiments, cells were trypsinized [Bergethon et al., 1989] then aliquoted into 6-well culture plates containing gelatin-coated circular glass slides, at a density of 7.5×10^4 cells per well, and allowed to spread to confluence. The cell environment was maintained at 37 °C throughout the study. External bath conditions for transmembrane potential studies were 1X Dulbecco's PBS containing 1.1 mmol/l Ca^{2+}. Because of the role of calcium flux in the signaling of NO, the NO response was studied under three extracellular Ca^{2+} conditions in PBS: 1) Ca^{2+} present (1.1 mmol/l); 2) Ca^{2+} present but Ca^{2+} channels blocked with 100 μmol/l Ni^{2+}; and 3) Ca^{2+} free.

Electric Stimulation

Sinusoidal alternating current waveforms were generated by a signal function generator (Circuitmate #FG2, Beckman Industrial, Brea, CA). This output signal was fed through a unity gain follower circuit constructed from an operational amplifier. Direct current (DC) stimulation was provided from a battery connected to a voltage divider circuit. All electric signals were routinely monitored by an oscilloscope (PCSU1000, Velleman, Richland Hills, TX) and digital multimeter (Fluke 8840, Optimum Energy Products, Calgary, Alberta, Canada) throughout each trial. Electrical stimulation was applied to the cell media via a pair of platinum electrodes, separated from the media by salt bridges formed from rectangular "plates" of poly-hydroxyethylmethacrylate (HEMA) hydrogel. These polymer hydrogel salt bridges were made according to the method of Kindler and Bergethon [1990]. In brief, HEMA hydrogels were prepared using a 1:1 volume:volume mixture of the HEMA monomer (S25464, Sigma Aldrich, St. Louis, MO) and 0.15 mol/l NaCl. The solution was degassed by vacuum on ice, and 0.1 ml of 12% sodium bisulfite and 0.1 ml of 6% ammonium persulfate (per 1 ml of monomer) was added to induce HEMA polymerization. Aliquots (5 ml) of solution were poured into 6 cm petri dishes, a platinum wire was placed into the central area of each dish, and polymerization proceeded in a humidified 37 °C incubator for 2 h.

Polymerization was complete when the clear solution became a flexible, white solid. Rectangular 0.5 cm × 2 cm electrode plates were cut out when polymerization was complete. Care was taken to ensure that the metal wires were securely encased in solid HEMA, with one end sticking out of the hydrogel plate. To remove the excess monomer, hydrogels were dialyzed with 0.15 mol/l NaCl over two weeks. Before use, the electrodes were sterilized by dipping the ends in 70% ethanol and allowing the ethanol to evaporate. The poly-HEMA-encased electrodes were placed on the right and left sides of the culture surface on the microscope stage. These integrated electrodes provided a sturdy, stable bridge that did not produce electrolytic contaminants and generated a uniform field across the BAEC monolayer (Fig.1).

Imaging System

A Nikon Eclipse E600N epifluorescent microscope (Tokyo, Japan) with a Diagnostic Instruments Spot Insight 2 18.0 Monochrome CCD camera (Sterling Heights, MI) was used to capture all images. An Xcite 120 light source (EXFO, Quebec, Canada) and a Nikon B-2E/C dichroic filter cube were used as the light source for the fluorescent dyes. Spot Software version 4.5.9.1 (Diagnostic Instruments) was used for all image acquisitions. ImageJ version 1.45c (National Institutes of Health (NIH), Bethesda, MD) was used for selecting regions of interest (ROIs) and all subsequent image processing The fluorescent dyes used in these studies showed no photobleaching under the conditions and instrumentation used in these studies.

Membrane potential studies

The membrane potential-sensitive fluorescent dye *bis*-(1,3-dibutylbarbituric acid)trimethine oxonol (DiBAC4(3); B438, Life Technologies) was used in these studies. The excitation and emission maxima are 490 nm and 516 nm, respectively, and the fluorescent signal increased with membrane depolarization. Calibration of the dye to membrane potential changes and resting membrane potentials of BAECs was determined using the null point method of He and Curry [1995]. Briefly, the BAEC monolayer was washed twice and bathed in Puck's Saline G (2917, Sigma Aldrich) containing 1 μmol/l DiBAC4(3) and was allowed to equilibrate for 1 h. An initial image (F_0) was acquired at an exposure of 500 ms. Gramicidin was added to a final concentration of 1 μmol/l. Following equilibration for 1 min, images were taken every 20 s for 5 min using the same exposure described above (F_i); thus, $\Delta F = (F_i - F_0)$. Experiments were repeated for four $[Na^+]_e$ levels (2, 8, 35, 110 mmol/l).

Measurement of the nitric oxide signal: Diaminofluorescein

For the direct measurement of intracellular nitric oxide (NO) production, BAECs were incubated with the membrane-permeant dye diaminofluorescein-2 diacetate [2-(3,6-diacetyloxy-4,5-diamino-9H-xanthen-9-yl)-benzoic acid] (DAF-2DA; 85165, Cayman Chemical, Ann Arbor, MI). DAF-2DA is uncharged and crosses the cell membrane into the cytoplasm where non-specific esterases remove the diacetate subgroups, thus rendering the molecule charged and trapped intracellularly. There, the non-fluorescent 4,5-diaminofluorescein (DAF-2) is available to react with locally produced NO or other products derived from the endothelial nitric oxide synthase (eNOS) system. When so exposed, DAF-2 binds with 2 molecules of NO to form the fluorescent product triazolofluorescein [Nakatsubo et al., 1998] with a wavelength of excitation at 485 nm and emission at 538 nm. In order to increase the constitutive NO production to levels above 5 nmol/l, 1 μmol/l of adenosine triphosphate (ATP) was added routinely to induce an observable amount of NO. L-arginine was added to a final concentration of 100 μM to all experimental solutions to provide excess substrate for the NO synthesis reaction. DAF-2 was calibrated using an NO donor molecule diethylenetriamine NONOate (DETA NONOate; 82120, Cayman Chemical) as described by Hrabie et al. [1993]. When this reaction occurs in the presence of cells pretreated with DAF-2DA, a positive control study can be conducted to calibrate the dye against known concentrations of NO [Keefer et al., 1996]. Below the 5 μmol/l concentration of DAF-2, a clear linear relationship between the NO in the cells and the fluorescence observed could be demonstrated. In this paper, the DAF-2 fluorescent response is called the “NO signal”. The elimination of the NO signal using the NO inhibitor l-nitroarginine methyl ester (L-NAME) [Moore et al., 1990] was shown in dose- dependent experiments with final L-NAME concentrations of 20, 50, 100, and 200 mmol/l. For these studies, we determined a dose-dependent effect that most consistently abolished the observed NO signal at 200 μmol/l. Abolition of the NO signal was demonstrated in independent controls for all experimental conditions described herein.

Background correction for the DAF-2 experiments used an inert no-light phantom (a small platinum block) to provide a baseline reference grey scale for no-light conditions. All post-processing included subtraction of this reference “no-light” condition. The background fluorescent noise from the DAF-2 was further suppressed by the routine addition of 0.4% (final concentration) trypan blue to the bathing solution. In addition to quenching non-specific fluorescence, trypan blue is a vital dye and provided a routine control to measure the viability of the assayed cells. Images were acquired at an exposure of 5 s, gain of 1, with one image taken every 5 min over a 2 h period. Post-processing was performed as described above with cell ROIs measured for integrated intensity over the area of the ROI, with the background subtracted from the phantom, and normalized with the equation: $(F_1\text{-}F_o)/F_o$.

Statistical Analysis

All data were tested for being normally distributed using the Shapiro-Wilk test. Statistical significance for normally distributed data was determined with the Student's unpaired t-test and one-way analysis of variance (ANOVA) to compare two groups, and three or more groups, respectively. Non-normally distributed data was tested for significance using the Kruskal-Wallis test. Probabilities of $p<0.05$ were considered significant. On each day that the experiments were conducted, three or more replicates were performed with the same experimental conditions. All experiments were repeated and the data presented is representative of these experiments. Statistical tests described above were used to determine if the means were equal for each time point. Means were calculated and data is presented as mean ± standard error of mean. The number of experiments (n) reflects number of replicates pooled together.

RESULTS

Membrane potential studies

All studies were performed with BAECs grown to confluence. The resting membrane potential of BAECs was determined to be −32±2 mV (Fig. 2). The slope of the linear calibration curve indicates a ratio of a 1 mV change in membrane potential to a 0.3 arbitrary unit change in observed normalized fluorescence (F_i-F_0/F_0). This proportionality constant was used for calculation of all subsequent membrane potential values.

The effects of isolated ELF electric fields on the BAEC membrane potential were studied by exposing confluent cells to fields with magnitudes and frequencies comparable to those expected under physiological conditions (from normotensive to hypertensive scenarios (for the cow 100–300 mm Hg systolic, i.e., 1.67 Vm^{-1} to 6.6 Vm^{-1}) and at normal heart rates (0.5–2 Hz) [Olson, 1971]. The EVSP field has both DC and alternating current (AC) components and these were studied separately. As Figure 3 demonstrates, when an ELF field is applied the BAECs undergo a steady-state depolarization that ranges between 1 and 8 mV compared to a field-free control. The BAEC depolarization is a function of both the field strength and frequency of the ELF: $\psi_m(E_{ELF}, \nu)$. Examination of Figure 3b shows that the degree of membrane depolarization is more heavily influenced by the frequency of the stimulation than by the field strength. In the presence of only a DC bias voltage, there is a very small but statistically significant depolarization on the order of 1 mV that shows no dependence on the field strength over the physiological range studied (Fig. 3a). In contrast to the depolarization seen at DC magnitudes, there is a more complex dependency of the endothelial cell resting membrane potential on field strength when a periodic field is applied. The BAECs show a threshold effect at 0.5 Hz, and then at a given frequency there is an apparent logarithmic relationship between the electric field magnitude and the depolarization effect seen in the endothelial cell membrane (Fig. 3b).

NO production studies

NO signal production in the BAECs was measured using the NO-sensitive fluorescent dye DAF-2DA. BAECs grown in culture have a very low level of constitutive NO production; therefore, a NO response was induced by stimulation with 1uM ATP. The NO response was studied under the three extracellular Ca^{2+} conditions (Ca^{2+} present (1.1 mmol/); Ca^{2+} present but Ca^{2+} channels blocked with 100 μmol/l Ni^{2+}; Ca^{2+} free).

NO production without ELF field exposure

ATP-stimulated BAECs in the presence of 1.1 mM extracellular Ca^{2+} produce a NO signal whose time course shows two clear phases (Fig. 4a): a logarithmic phase that reaches maximum within 30 min of the ATP stimulation (Fig. 4b); and an exponential phase that

becomes noticeable at 30 min and continues for the duration of the experiment (Fig. 4c). Each of these ATP-induced phases can be separated by altering the Ca^{2+} conditions either by $NiCl_2$ treatment or removal of extracellular Ca^{2+}. Figure 3d shows that the $NiCl_2$ blockade eliminates the later exponential process while the earlier logarithmic process is unaffected by this treatment. In the absence of extracellular Ca^{2+}, an increase in the NO signal compared to control is not seen with either the clear logarithmic or the exponential phase.

NO production in the presence of the ELF field

The relationship of the NO signals to the ELF field could be differentiated by changes in the early (logarithmic) and later (exponential) phases. Under the condition of 1.1 μM extracellular Ca^{2+} (Fig. 5a), the logarithmic process is potentiated in an amplitude-dependent fashion (proportional to the field; Fig. 5b), and the exponential process is unchanged with respect to the unstimulated cells (Fig. 5c).

Figure 6 (a and b) shows that in the Ca^{2+}-free solution, the ELF field increases only the exponential phase of NO production in an amplitude- and frequency-dependent manner. Observations made during stimulation in the Ni^{2+} blockade condition (Fig. 6c) show an essential elimination of the early phase potentiation seen in Figure 5b. The late phase NO signal is not eliminated under the Ni^{2+} blockade and has a field strength dependency.

DISCUSSION

These studies show that the biological response to ELF and low-magnitude electric fields on the order expected *in vivo* from the EVSP is an independent physical factor that influences endothelial cell electrophysiology and NO production. We asked what effect the isolated EVSP electrical field would have on the BAEC membrane potential. Though there is a net steady-state DC component to the flow of blood through the blood vessel, another feature of the vascular flow in a blood vessel is a pulsatile component seen throughout the arterial tree. We reasoned that this AC component was likely the dominant biological feature produced by the electrokinetic effect because previously an electroconformational coupling mechanism of EVSP–cell interaction had been postulated in the vascular smooth muscle cell [Bergethon, 1991]. Therefore, we predicted that the membrane potential change induced by the EVSP-level ELF field would be dependent on the frequency of the applied field. Our results confirmed both a frequency effect at normal physiological and tachycardic rates of pulsatile flow (2 Hz) and also an additional effect of field magnitude. The resulting effects lead to the suggestion of a “tuning curve” in which the field strength may rise to a maximum biological effect and then fall off. Thus, electrical fields of biological character cause a graded membrane depolarization that is dependent on variables that are clinically relevant (blood pressure and pulse rate).

We investigated the hypothesis that these ELF fields are a control factor in broader vascular biology and therefore postulated an effect on NO production. The membrane potential in the endothelial cell plays an important role in modulating Ca^{2+} signaling, which is an essential control system for the production of NO from the endothelial cell. Thus, while recognizing that the molecular target(s) of these ELF fields are unknown and could be intracellular as well as membrane localized, we hypothesized that field exposure would decrease NO production by BAECs because the demonstrated depolarization of the endothelial cell would reduce the Ca^{2+} flux into the cells.

Because the working hypothesis was that the production of NO would be directly proportional to the magnitude of the BAEC membrane polarization, we predicted that the NO signal from DAF-2 would be reduced on exposure to the EVSP-character field. Because

BAECs grown in culture have a very low level of constitutive NO production, we thought it necessary to induce a large enough NO response so that it could be suppressed. Therefore, BAECs were activated by treatment with 1 μM ATP.

The early logarithmic phase of NO production followed by the exponential phase, demonstrated in Figure 3, has been reported previously on ATP stimulation or Ca^{2+} ionophore stimulation [Corson et al., 1996]. The early log phase is associated with intracellular Ca^{2+}-mediated transients with a sustained NO production dependent on the later phase associated with Ca^{2+} flux down the Nernstian gradient. We attempted the dissociation of these two ATP-induced phases by the elimination of Ca^{2+} flux from the extracellular to intracellular compartments by $NiCl_2$ blockade of T- and L-type calcium channels. The persistence of the logarithmic phase but the abrogation of the exponential phase supports a model in which the initial NO signal response to ATP occurs as a result of the release of intracellular stores of Ca^{2+}. The exponential phase is dependent on the flux of Ca^{2+} from the extracellular to intracellular compartments. The role of Ca^{2+} flux in the early phase is known [Nilius and Droogmans, 2001] and this effect can be seen in Figure 3d by comparing the initial phases with the Ni^{2+} blockade to the case in which extracellular Ca^{2+} is removed. Thus, our experimental model is sensitive to a variety of pathways leading to NO production in BAECs and was used to parse a description of ELF electric field targeting.

With these phases in mind, the hypothesis that the field-induced depolarization would be an attenuating force on Ca^{2+} flux was refined to posit an attenuation on the exponential phase of the ATP-stimulated NO signal. Surprisingly, the experiments in which BAECs were exposed to EVSP-type fields showed a strong enhancing effect of the ELF field on the NO signal associated with early intracellular processes while the hypothesized elimination of the Ca^{2+} flux-associated NO production was not demonstrated. While an EVSP-type effect on the NO signal can be demonstrated, it is not simply tied to the depolarization effect on the BAECs. Since ELF fields are expected to cause depolarization under these conditions and NO is not decreased suggests several sites of action of the ELF field on the pathways responsible for producing the NO signal in the presence of extracellular Ca^{2+}. These sites remain to be identified.

Finally, the experiments in the Ca^{2+}-free solution with the ELF electric stimulation show only increases in exponential NO production in an amplitude- and frequency-dependent manner. This suggests that in the late phase the field acts on a target that potentiates NO production without requiring Ca^{2+} flux. The Ca^{2+}-free condition supports the postulate that the late phase targets are not simply reflecting the Ca^{2+} flux and are likely independent of the electrophysiological effects associated with the altered membrane potential. Observations made during ELF electric field stimulation in the Ni^{2+} blockade condition support that there are multiple targets of the field (Fig. 5c). The Ni^{2+} blockade essentially eliminated the early phase potentiation (Fig. 4b), suggesting that surprisingly, the likely target of the field in the early phase is a mechanism involving Ca^{2+} flux via a Ni^{2+} blockable channel. Alternatively, a novel biophysical interaction between an ELF electric field and a purinergic receptor complex that can be blocked with Ni^{2+} may be postulated. The late phase NO signal is not eliminated under the Ni^{2+} blockade but has a field strength dependency that suggests a target that is not related to Ca^{2+} flux.

These studies demonstrate complex and physiologically important effects on BAECs from electric fields at the levels associated with vascular blood flow in the mammalian vasculature. An important role for EVSP-type ELF fields as a control factor in endothelial cell function and vascular biology is thus well supported through both biological and biophysical mechanisms; however, the multiple specific targets of action remain to be elucidated. The likely mechanism that links these fields to cellular effects is the

electroconformational coupling of an applied periodic electric field to membrane-associated processes, which has been established both theoretically and experimentally [Serpersu and Tsong, 1984; Astumian et al., 1989].

Some speculation on the clinical implications of the EVSP on endothelial cells might be offered. The amplitude of the EVSP field varies proportionally to blood pressure, and the zeta potential reflects the integrity of the vascular interface with the blood. The EVSP changes when the vessel surface is altered, which occurs in atherosclerotic plaque formation and as blood pressure rises and falls. A dissociation of the shear force and the EVSP may play a role in endothelial cell activity in areas of turbulence (e.g., following vessel narrowing from atheromatous plaque) since in these regions the shearing force falls dramatically while the EVSP would remain, leading to a region of smooth muscle cell depolarization that may act to depolarize and cause vasoconstriction of local smooth muscle cells. In addition, the pulsatile flow that leads to a varying periodic field is attenuated in regions of turbulence leading to a lower frequency of the EVSP. The homeostasis between the shearing force and the EVSP may be altered in areas of turbulence with a reduction in NO production because of reduced shear and reduced EVSP local frequency. Another finding of some significance comes from our own evaluation of arterial pulse tracings during acute hypertension and hypertensive crisis (data not shown). The arterial pulse in normotension is characterized by a sinusoidal shaped wave on the upstroke that decays with a somewhat flatter downstroke and then provides a steady-state wave during the remainder of diastole. During hypertension, the upstroke is much more pronounced and there is a diastolic waveform in which two other well-formed sinusoidal waves appear. The EVSP wave function thus triples under these conditions, and combined with the amplitude tuning curve shown earlier, suggests a complex biological response that needs further study. Lastly, the ELF fields of EVSP character affect both the endothelial cell and the smooth muscle cell independently, as this and other work has shown. The possibility of vascular cell interactions co-modulated by ELF electric fields opens further questions about vascular homeostasis and pathobiology. All of these factors are important considerations in new vascular biophysics and biochemistry studies of the blood vessel that should now include ELF electric fields such as the EVSP.

Acknowledgments

Grant sponsors: NIH (National Institute of Aging); Grant number: T32-AG00277 (to DPT); Boston University School of Medicine (to PRB).

REFERENCES

Adams DJ, Barakeh J, Laskey R, Van Breemen C. Ion channels and regulation of intracellular calcium in vascular endothelial cells. FASEB J. 1989; 3:2389–2400. [PubMed: 2477294]

Astumian RD, Robertson B. Nonlinear effect of an oscillating electric field on membrane proteins. J Chem Phys. 1989; 91:4891–4901.

Augustin-Voss HG, Voss AK, Pauli BU. Senescence of aortic endothelial cells in culture: Effects of bFGF expression on cell phenotype, migration and proliferation. J Cell Physiol. 1993; 157:279–288. [PubMed: 8227161]

Bergethon PR. Altered electrophysiologic and pharmacologic response of smooth muscle cells on exposure to electrical fields generated by blood flow. Biophys J. 1991; 60:588–595. [PubMed: 1932549]

Bergethon PR, Trinkaus-Randall V, Franzblau C. Modified hydroxyethylmethacrylate hydrogels as a modeling tool for the study of cell-substratum interaction. J Cell Sci. 1989; 92:111–121. [PubMed: 2777911]

Corson MA, James NL, Latta SE, Nerem RM, Berk BC, Harrison DG. Phosphorylation of endothelial nitric oxide synthase in response to fluid shear stress. Circ Res. 1996; 79:984–991. [PubMed: 8888690]

Cunningham KS, Gotleib AI. The role of shear stress in the pathogenesis of atherosclerosis. Lab Invest. 2005; 85:9–23. [PubMed: 15568038]

Falk E. Pathogenesis of atherosclerosis. J Am Coll Cardio. 2006; 47:C7–C12.

He P, Curry FE. Measurement of membrane potential in endothelial cells in single perfused microvessels. Microvascular Res. 1995; 50:83–198.

Hrabie JA, Klose JR, Wink DA, Keefer LK. New nitric oxide-releasing zwitterions derived from polyamines. J Org Chem. 1993; 58:1472–1476.

Kang H, Fan Y, Deng X. Vascular smooth muscle cell glycocalyx modulates shear-induced proliferation, migration and NO production. Am J Physio Heart Circ Physio. 2011; 300:H76–H83.

Keefer LK, Nims RW, Davies KM, Wink DA. NONOates (1-substituted diazen-1-ium-1,2-diolates) as nitric oxide donors: Convenient nitric oxide dosage forms. Meth Enzymol. 1996; 268:281–293. [PubMed: 8782594]

Kindler DD, Bergethon PR. Non-toxic and durable salt bridges using hydroxyethylmethacrylate hydrogels. J Appl Physiol. 1990; 69:373–375. [PubMed: 2394659]

Li YJ, Haga JH, Chien S. Molecular basis of the effects of shear stress on vascular endothelial cells. J Biomech. 2005; 38:1949–1971. [PubMed: 16084198]

Lieu DK, Pappone PA, Barakat AI. Differential membrane potential and ion current responses to different types of shear stress in vascular endothelial cells. Am J Physiol Cell Physiol. 2004; 286:C1367–C1375. [PubMed: 14761889]

Moore PK, Al-Swayeh OA, Chong NS, Evans RA, Gibson A. L-NG-nitro-arginine, a novel L-arginine reversible inhibitor of endothelium-dependent vasodilation in vitro. Br J Pharmacol. 1990; 99:408–412. [PubMed: 2328404]

Nakatsubo N, Kojima H, Kikuchi K, Nakatsubo N, Kojima H, Kikuchi K, Nagoshi H, Hirata Y, Maeda D, Imai Y, Irimura T, Nagano T. Direct evidence of nitric oxide production from bovine aortic endothelial cells using new fluorescence indicators: Diaminofluoresceins. FEBS Letters. 1998; 427:263–266. [PubMed: 9607324]

Nilius B, Droogmans G. Ion channels and their functional role in vascular endothelium. Physiol Rev. 2001; 81:1415–1459. [PubMed: 11581493]

Noris M, Morigi M, Donadelli R, Aiello S, Foppolo M, Todeschini M. Nitric oxide synthesis by cultured endothelial cells is modulated by flow conditions. Circ Res. 1995; 76:536–543. [PubMed: 7534657]

Olsen JD. Periodic elevations of blood pressure of cattle during exposure to subzero environmental temperatures. Int J Biometeor. 1971; 15:225.

Quincke G. Ueber die fortführung materieller theilchen durch strömende elektricität (On the continuation of material particles by the flow of electricity). Ann Phys. 1861; 189:513–598.

Roger VL, Go AL, Lloyd-Jones DM, Adams RJ, Berry JD, Brown TM. Heart disease and stroke statistics-2011 update. Circulation. 2011; 123:e18–e209. [PubMed: 21160056]

Sawyer PN, Himmelfarb E, Lustrin I, Ziskind H. Measurement of streaming potentials of mammalian blood vessels, aorta and vena cava, in vivo. Biophys J. 1966; 6:641–651. [PubMed: 5970567]

Schwartz CJ, Valente AJ, Sprague EA, Kelley JL, Nerem RM. The pathogenesis of atherosclerosis: An overview. Clin Cardiol. 1991; 14:I1–I16. [PubMed: 2044253]

Serpersu EH, Tsong TY. Activation of electrogenic Rb^+ transport of (Na,K)-ATPase by an electric field. J Biol Chem. 1984; 259:7155–7162. [PubMed: 6327708]

Voets T, Droogmans G, Nilius B. Membrane currents and the resting membrane potential in cultured pulmonary artery endothelial cells. J Physiol. 1996; 497:95–107. [PubMed: 8951714]

World Health Organization. Geneva, Switzerland: WHO; 2011. The atlas of heart disease and stroke: Cardiovascular disease. Fact sheet No. 317. http://www.who.int/mediacentre/factsheets/fs317/en/index.html

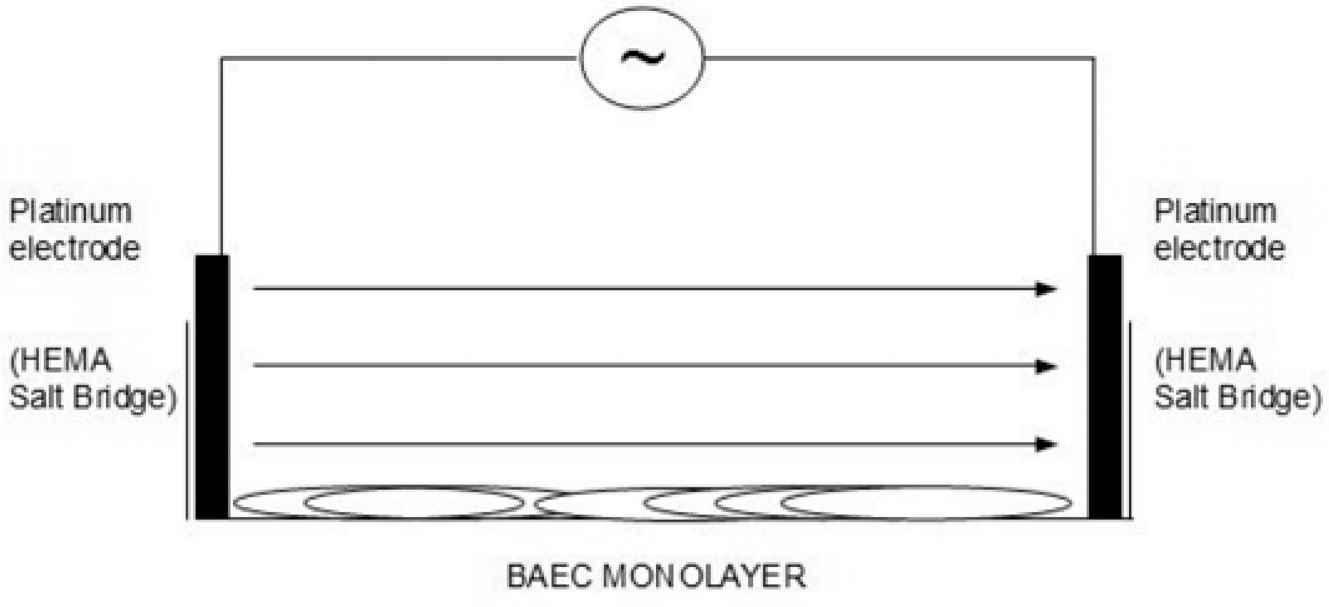

Figure 1.
Diagram of apparatus for bovine endothelial cell monolayer electric stimulation.

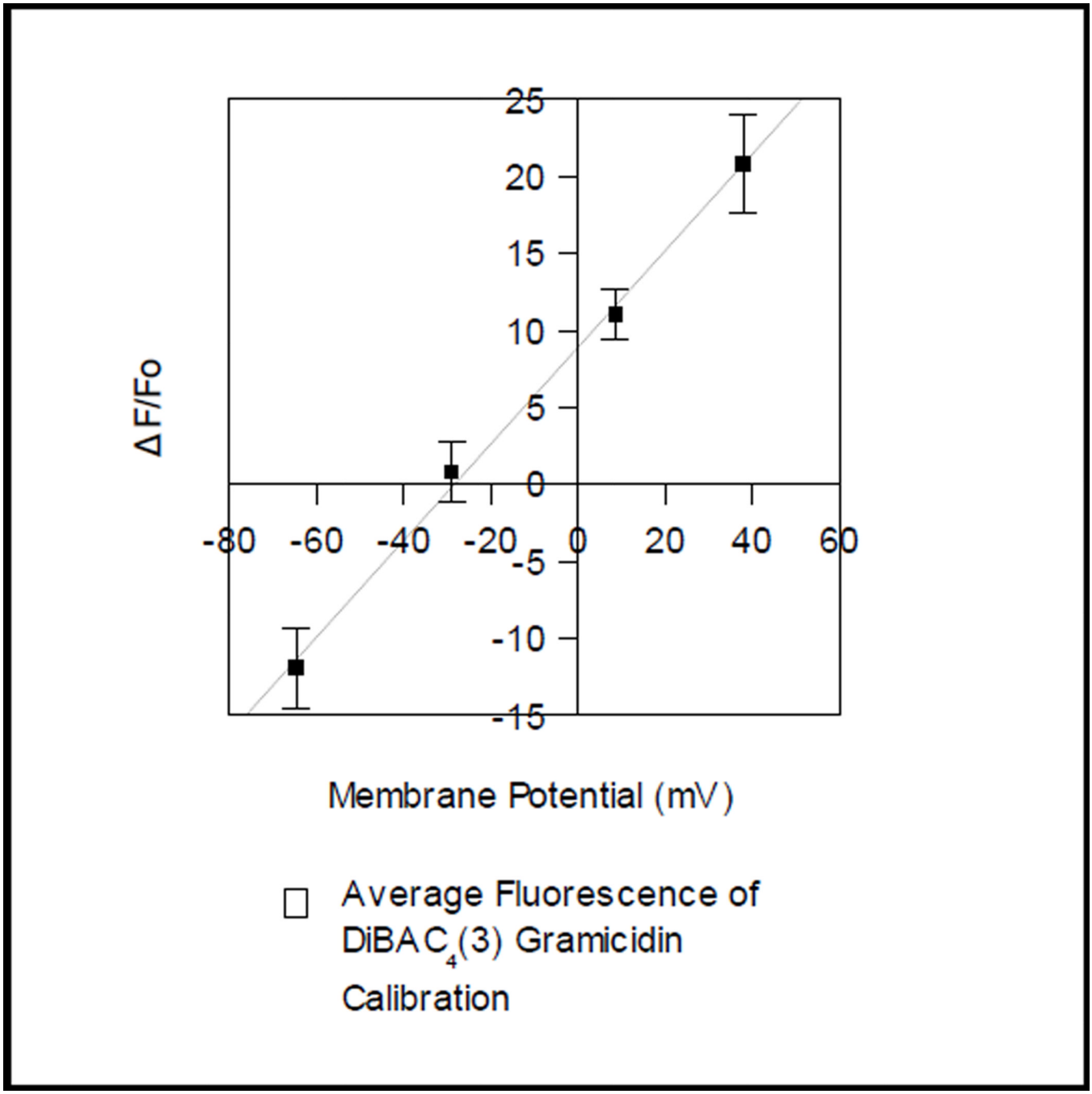

Figure 2.
DiBAC4(3) calibration curve. Equation for best-fit line: ΔF/F0=0.3(Ψ) + 8.98 (n=6). The x-intercept (ΔF/F0 = 0) is the resting membrane potential of the BAECs.

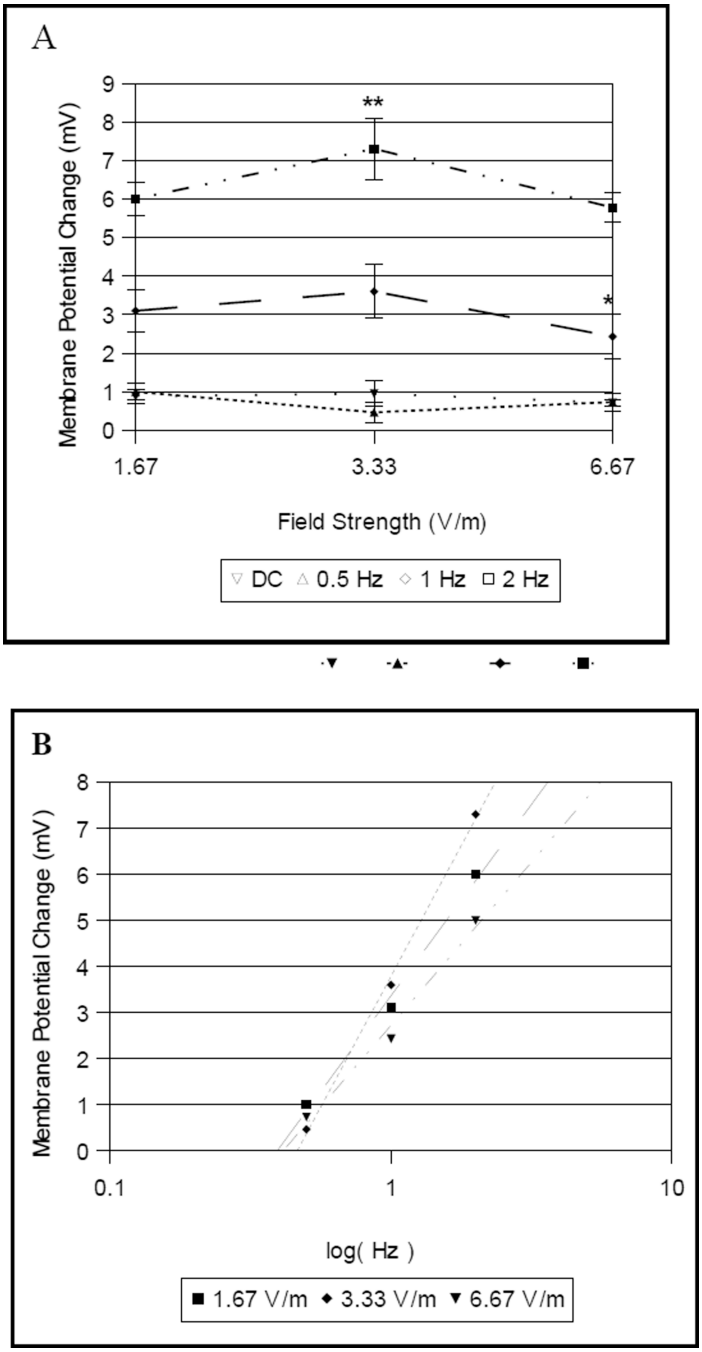

Figure 3.

EVSP-induced frequency-dependent depolarization. (A): Direct current (n=6) and 0.5 Hz (n=6) stimulation show no significant difference at the three field strengths (1.67 V/m, p=0.35; 3.33 V/m, p= 0.08; 6.67 V/m, p=0.42). At 1 Hz stimulation (n=9), a ~ 3 mV depolarization occurs, (*) with a lower depolarization at 6.67 V/m (vs. 1.67 V/m, p = 0.01; vs. 3.33 V/m, p = 0.02). At 2 Hz stimulation (n=9), a ~6 mV depolarization occurs, (**) with a higher depolarization at 3.33 V/m (vs. 1.67 V/m, p=0.001; vs. 6.67 V/m, p=0.0001). (B): Equations for best-fit lines: 1.67 V/m, $3.61\times\ln(t)+3.37$, $R^2=0.99$; 3.33 V/m, $4.93\times\ln(t)+3.79$, $R^2=0.99$; 6.67 V/m, $3.08\times\ln(t)+2.72$, $R^2=0.99$.

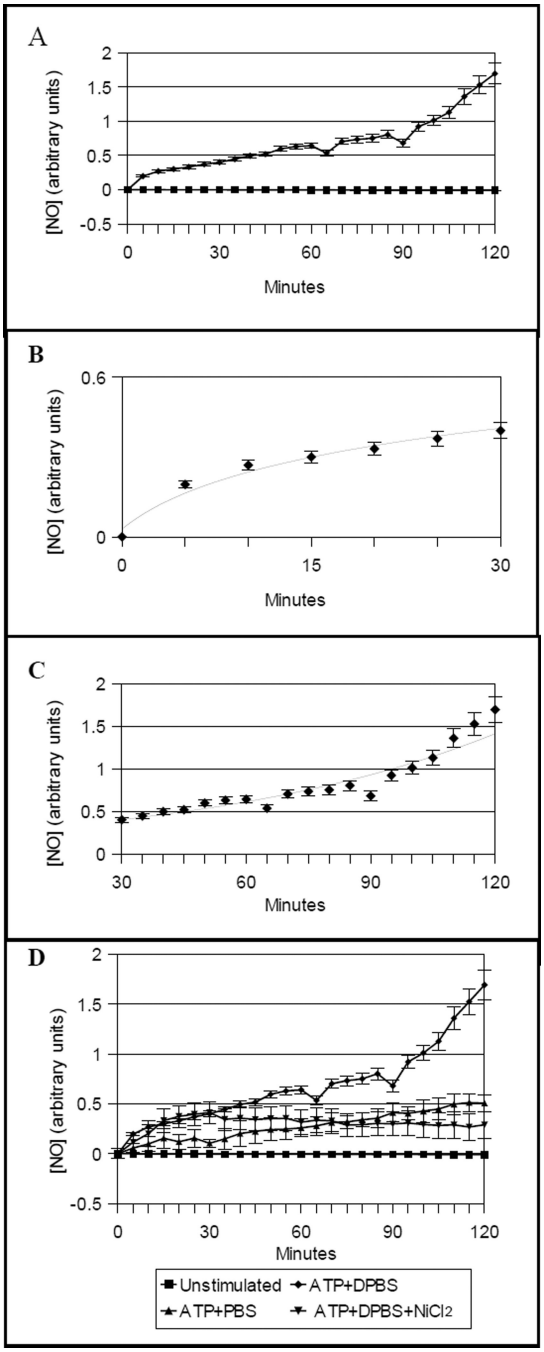

Figure 4.

NO signal with ATP stimulation and varying calcium conditions without electric stimulation. (A): NO signal in the presence of Ca^{2+}. (B): Early logarithmic phase during the first 30 min of (A). Equation for best-fit line: NO=0.20×1n(t))+0.03, R^2=0.97. (C): A late exponential phase seen in the final 90 min. Equation for best-fit line: NO=0.434×$e^{(0.134t)}$, R^2=0.99. (D): ATP stimulation with [Ca^{2+}]e (n=3) and ATP stimulation without [Ca^{2+}]e (n=4) or with calcium channel blockade (n=3).

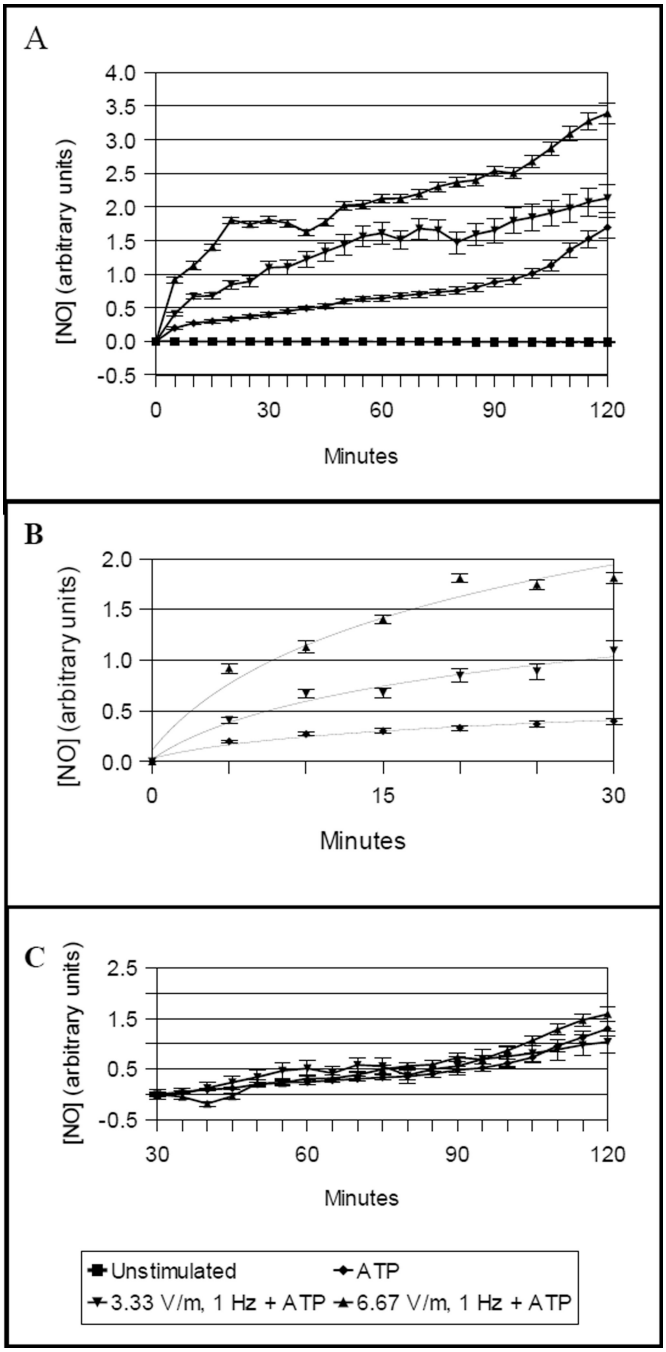

Figure 5.

EVSP effect on the NO signal in the presence of 1.1 mM $[Ca^{2+}]e$. (A): Unstimulated control (n=3) and ATP stimulation (n=3) and EVSP+ATP stimulation at 3.33 V/m (n=3) and 6.67 V/m (n=3).

(B): Relationship of early log phase to EVSP field strength. Equations of best-fit lines: ATP only, NO= 0.20×ln(t) + 0.03, R^2 = 0.97; 3.33 V/m + ATP, NO=0.52×ln(t)+0.02, R^2 = 0.98; 6.67 V/m + ATP, NO=0.94×ln(t)+0.11, R^2=0.97. (C): Exponential phases of the three curves with the log phase value at t=30 min subtracted.

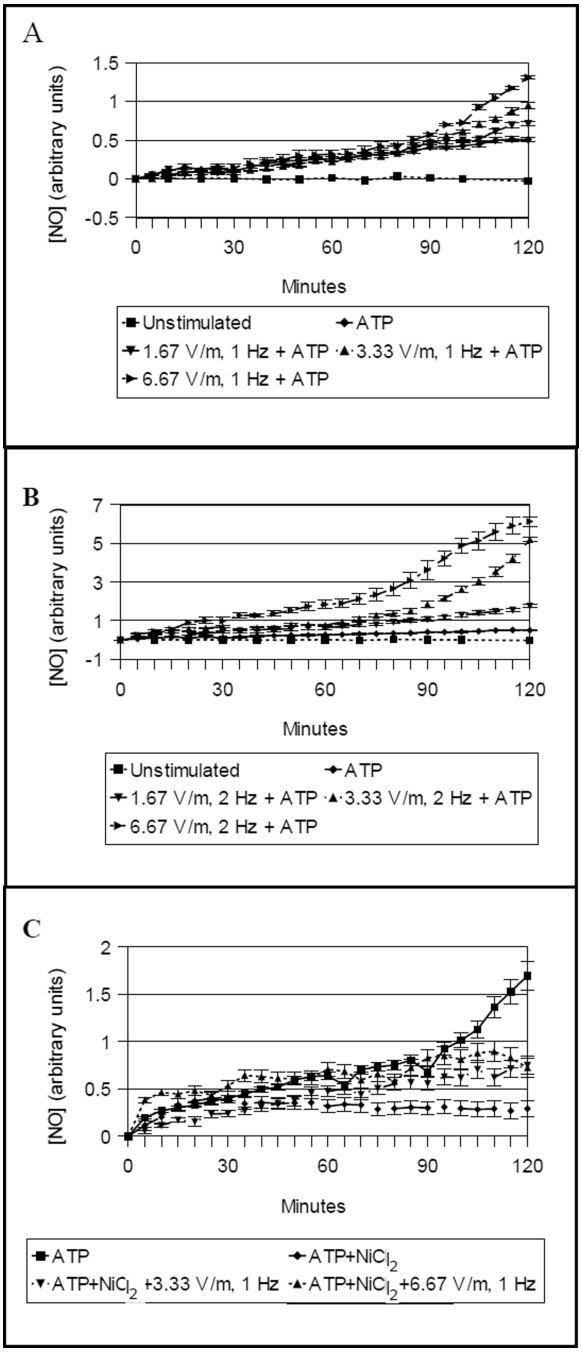

Figure 6.

EVSP effect on the NO signal in Ca^{2+}-free and calcium channel-blocked conditions. Unstimulated (n=3), ATP only (n=4), 1.67 V/m + ATP (n=3), 3.33 V/m + ATP (n=3), and 6.67 V/m + ATP (n=3) at (A): 1 Hz and (B): 2 Hz. (C): EVSP stimulation with the $NiCl^2$ blockade (n=3), 3.33 V/m +ATP (n=2), and 6.67 V/m +ATP (n=2).